Molecular Science

AIMS Molecular Science, 13(1): 80–96.
DOI: 10.3934/molsci.2026005
Received: 13 October 2025
Revised: 28 January 2026
Accepted: 02 February 2026
Published: 03 March 2026

https://www.aimspress.com/journal/Molecular

Research article

Molecular mechanisms of enhanced apoptosis in hepatocellular carcinoma via cantharidin-loaded liposomes

Ruihua Duan[1,#], Jiao Dong[2,#], Mingjie Chen[3,#], Caixia Huang[4,#], Shenglong Gan[5], Runcong Liu[4], Ronghuan Yang[4], Hao Li[2,*], Zhoulei Li[3,6,7,*] and Yisheng Lin[4,*]

[1] Department of Medical Imaging, Maternal and Child Health Hospital of Hubei Province, Wuhan, Hubei 430070, China
[2] South China Academy of Advanced Optoelectronics, South China Normal University, Guangzhou, Guangdong 510006, China
[3] Department of Radiology, The First Affiliated hospital, Sun Yat-Sen University, 58 Zhongshan II Road, Guangzhou, Guangdong 510080, China
[4] Department of Interventional Radiology, Huizhou Central People's Hospital, Huizhou Guangdong 516001, China
[5] Shenzhen Medical Academy of Research and Translation, Shenzhen Guangdong 518107, China
[6] Department of Radiology, The Second Affiliated Hospital of Guangzhou University of Chinese Medicine, Guangzhou, China
[7] Guangzhou Xinhua University, Guangzhou 510520, China

[#] These four authors contributed equally to this work.

[*] **Correspondence:** Email: haoli@m.scnu.edu.cn; zhoulei.li@hotmail.com; yisheng.lin@163.com.

Abstract: Objective: Hepatocellular carcinoma (HCC) remains a molecularly complex malignancy with limited therapeutic options. Cantharidin (CTD), a natural terpenoid, exhibits potent antitumor activity but suffers from poor bioavailability and dose-limiting toxicity. This study aimed to develop CTD-loaded liposomes (CTD-Lips) and investigate their molecular mechanisms in enhancing apoptosis and cell cycle regulation in HCC. **Methods:** CTD-Lips were prepared using an optimized thin-film method and thoroughly characterized for size, encapsulation efficiency, and drug release profile. Cellular uptake was evaluated using coumarin-6-loaded nanoparticles in HepG2 cells. Cytotoxicity was assessed by CCK-8 assay, while apoptosis and cell cycle distribution were analyzed via flow cytometry. In vivo antitumor efficacy and systemic safety were evaluated in HepG2-

xenografted nude mice compared to cisplatin, with comprehensive histopathological and biochemical analyses. **Results:** Optimized CTD-Lips showed nanoscale characteristics (120.80 nm) with high encapsulation efficiency (96.20%) and sustained release. Cellular uptake was significantly enhanced, leading to superior cytotoxicity (IC_{50}: 1.415 μg/mL vs. 4.971 μg/mL for free CTD) and induced S-phase cell cycle arrest. Molecular analysis revealed that CTD-Lips promoted apoptosis through enhanced DNA damage response. In vivo, CTD-Lips achieved 62.4% tumor growth inhibition, outperforming cisplatin, while maintaining systemic safety with no significant hematological or biochemical alterations. **Conclusions:** CTD-Lips represent a molecularly targeted nanoplatform that enhances CTD's antitumor efficacy through regulation of cell cycle progression and apoptosis pathways. This study provides molecular-level insights into CTD-Lip-mediated anticancer mechanisms, supporting its potential as a novel molecular-targeted therapy for HCC.

Keywords: molecular targeted therapy; apoptosis; cell cycle; liposomes; hepatocellular carcinoma; nanomedicine; cantharidin

1. Introduction

Hepatocellular carcinoma (HCC) persists as a major global health burden, ranking among the leading causes of cancer-related mortality worldwide. Despite advancements in therapeutic strategies encompassing surgical resection, locoregional interventions, molecularly targeted agents, and immunotherapy, the overall prognosis for HCC patients remains suboptimal. Significant challenges, including high rates of tumor recurrence, the development of chemoresistance, and substantial treatment-associated toxicities, continue to underscore the urgent need for novel and more effective therapeutic entities [1].

Cantharidin (CTD), a natural bioactive sesquiterpenoid derived from the traditional Chinese medicinal insect *Mylabris phalerata* (Pallas), has garnered considerable attention for its broad-spectrum antitumor properties [2]. Compelling pharmacological evidence has demonstrated CTD's efficacy against a diverse array of malignancies, including hepatic, oral, pancreatic, gastric, mammary, and pulmonary carcinomas [3–9]. Its anticancer activity is primarily attributed to the modulation of critical molecular pathways, such as the inhibition of protein phosphatase 2A (PP2A), induction of DNA damage, and regulation of key signaling cascades including JAK2/STAT3 and PI3K/Akt, ultimately leading to cell cycle arrest and apoptosis [10–14]. However, the clinical translation of CTD has been severely hampered by its inherent physicochemical and pharmacological drawbacks. These include extremely poor aqueous solubility, low oral bioavailability, a narrow therapeutic window, and dose-limiting nephrotoxicity and gastrointestinal complications, which collectively restrict its utility in clinical oncology [15].

Nanotechnology-based drug delivery systems, particularly liposomes (Lips), have emerged as a promising strategy to overcome the limitations of conventional chemotherapeutic agents. Liposomes offer distinct advantages such as enhanced drug encapsulation efficiency, improved biocompatibility, controlled release profiles, and the potential for passive tumor targeting via the enhanced permeability and retention (EPR) effect [16–19]. These characteristics make liposomes an ideal platform for the delivery of challenging molecules like CTD, potentially augmenting its therapeutic index by improving solubility, prolonging systemic circulation, and reducing off-target toxicity.

Building upon this rationale, the present study aimed to develop and evaluate cantharidin-loaded liposomes (CTD-Lips), with a primary focus on their in vitro and in vivo antitumor efficacy. We hypothesized that encapsulating CTD in liposomes would enhance its delivery to hepatocellular carcinoma cells and amplify its pro-apoptotic and cell cycle disruptive effects with improvement of antitumor activity. This work seeks to lay a scientific foundation for exploring CTD-Lips as a potential novel therapeutic for hepatocellular carcinoma.

2. Materials and methods

2.1. Animals and ethics approval of research

The animal model of HCC was established using 5–6-week-old BALB/c-nu mice. Animal experiments were reviewed and approved by the Ethics Committee of Guangzhou University of Chinese Medicine (approval number: 20221017002).

2.2. Preparation of cantharidin liposomes

For the preparation of CTD-Lips, 7 mg of cantharidin, 50 mg of egg yolk lecithin, and 25 mg of cholesterol (Shanghai Chuangsai Technology Co., Ltd.) were completely dissolved in 30 mL of chloroform. Mannitol was used as a cryoprotectant during lyophilization to maintain particle integrity and prevent aggregation. The solvent in the mixed solution was then removed by rotary evaporation under reduced pressure at 50 ℃, resulting in the formation of a uniform light-yellow film on the wall of the round-bottom flask. Subsequently, mannitol aqueous solution was added, and hydration was achieved using a magnetic stirrer at a speed of 1000 rpm. Probe sonication was performed at 220 W for 10 min (5 s on, 5 s off cycles) in an ice bath to prevent overheating. The suspension was passed 10 times through a 220 nm polycarbonate membrane to achieve a uniform particle size. The formulation strategy utilized lecithin and cholesterol as solid matrix-forming lipids, and the combined sonication extrusion steps ensured the formation of solid-core nanoparticles with consistent nanosized characteristics.

2.3. Characterization of CTD-Lip

To characterize the CTD-Lip, the particle size, polydispersity index (PDI), in vitro release, and zeta potential distribution were determined using a Zetasizer Nano ZS90 analyzer (Malvern Instruments Ltd., Great Malvern, UK). Subsequently, the particle size and morphology of liposomes were measured using transmission electron microscopy (HITACHI Ltd., Tokyo, Japan), and photographs were taken.

Encapsulation efficiency (EE%) was calculated as the proportion of the drug encapsulated in liposomes compared to the total amount of CTD (M_{total}) present in the liposome preparation. Subsequently, a low-temperature and low-speed centrifugation method was utilized for the separation of nanoparticles and free drugs. Specifically, 1 mL of CTD-Lip solution was pipetted into a 10-mL volumetric flask with 9 mL of chromatography-grade methanol. The resulting mixture was shaken thoroughly until complete dissolution occurred. After mixing, peak area A1 was measured at a wavelength of 230 nm, and the standard curve equation was applied to calculate sample concentration

C1 and volume V1 (Thermo Scientific HPLC system, USA). Then, 1 mL of CTD-Lip suspension underwent centrifugation at 3000 rpm for 5 min in a centrifuge tube, and 1 mL of supernatant was collected and brought up to a fixed volume with ultrasonic demulsification before being dissolved through shaking using a 0.45 μm filter membrane. The filtrate underwent detection according to the above chromatographic conditions. Subsequently, peak area A2 was obtained using the standard curve equation applied to determine supernatant sample concentration C2 and volume V2. Finally, a formula to calculate EE% was applied using the samples' concentration data (C1 and C2) as well as their volumes (V1 and V2). The drug loading (DL) was calculated as the ratio of the amount of drug in the liposomes to the weight of the CTD-Lips. To do so, the quality of lyophilized powder samples containing CTD-Lip was measured and recorded as M, before being added to methanol for dissolution purposes, while HPLC (Thermo Scientific, United States) detected CTD content W0.

$$EE\%=(C2\times V2)/(C1\times V1)\times 100\% \quad (1)$$

$$DL\%=(W0/M_{total})\times 100\%$$

Dialysis tubing was employed to investigate the in vitro release of CTD-Lip; 4 mL of CTD-Lip and an equivalent amount of CTD were utilized as controls, which were then placed inside a pre-treated dialysis tube (molecular rejection of 3.5 kDa). The release medium (PBS, pH 6.8) and volume (16 mL) were selected to ensure the concentration of released cantharidin remained well below 10% of its saturation solubility throughout the experiment, followed by incubation in a constant temperature shaking water bath at 37 °C and 100 rpm for different time intervals: 1, 2, 4, 6, 8, 12, 24, 36, and 48 h, respectively. At each time point, a sample volume of 2 mL was withdrawn while simultaneously adding an equal volume of isothermal blank release medium. The cumulative release percentage at various time points was determined through HPLC measurement and analysis.

2.4. Cell uptake and cytotoxicity assay

According to the preparation method outlined in section 2.2, Coumarin 6 (C6), the fluorescent dye, was encapsulated within nanoparticles to obtain C6-Lip. Subsequently, C6-Lip and free C6 were co-incubated with human hepatocellular carcinoma HepG2 cells at a concentration of 5 μg/mL for 1, 2, 4, and 6 h. Cells were then fixed using a solution of 4% paraformaldehyde and stained with DAPI-containing anti-fluorescence quencher to visualize the nucleus. Fluorescence microscopy was employed to observe cellular uptake of fluorescence, followed by image collection.

To determine the cytotoxicity of CTD-Lip on HCC cells, the concentrations of CTD and CTD-Lips were determined to be 0.45, 0.9, 1.8, 3.6, 7.2, 14.4, and 28.8 μg/mL using CCK-8 (Guangzhou Jiayan Biotechnology Co., Ltd., Guangzhou, China). The blank control (liposomes only) was prepared at equivalent lipid concentrations of 25, 50, 100, 200, 400, and 800 μg/mL (n = 6) per concentration group. Blank control group and zeroed wells were also included simultaneously for comparison purposes.

After co-incubation with HepG2 cells for 24 h, the culture medium was discarded, followed by the addition of 10 μL of CCK-8 solution to each well for further incubation for 1 h. Subsequently, the absorbance value (OD) at a wavelength of 450 nm was measured using a microplate reader (Thermo Fisher Scientific China Co., Ltd.). Finally, the cell viability as well as the IC_{50} value were calculated.

2.5. Cell cycle and apoptosis assays

The CTD-Lip group, blank control (liposomes only), and free control (without any treatment) group were established separately. The administration group had a CTD concentration of 1.42 μg/mL. After administration, cells were cultured in an incubator for 24 h for cell cycle analysis. For the apoptosis assay, HepG2 cells were cultured for an additional 48 h in the incubator. Subsequently, the cells were digested and collected to create a single-cell suspension and were washed twice with pre-chilled PBS and subjected to AnnexinV/PI kit (Guangzhou Ruishu Co., Ltd., Guangzhou, China) according to the provided protocol for analysis by BD flow cytometer (Franklin Lake, New Jersey, USA).

2.6. Evaluation of anti-cancer efficacy in vivo

HepG2 cells in the logarithmic growth phase were harvested and subjected to three washes with trypsin and PBS. Subsequently, 100 μL of cell suspension (containing approximately 2×10^7 cells) was subcutaneously inoculated into the left axillary region of nude mice. Once visible subcutaneous tumors developed in the mice, their body weight was measured using an electronic balance, while the length and width of the tumor were recorded using vernier calipers every other day. Simultaneously, the volume (V) of each tumor was calculated as follows:

$$V = (\text{length} \times \text{width} \times \text{width})/2.$$

When the subcutaneous tumor volume of nude mice reached approximately 100 mm^3, the mice were randomly divided into three groups (n = 5): a normal saline group (C1), a positive drug comparison group (DDP: C2), and a CTD-Lip group (Tx). The dosage of the positive drug (cisplatin) was converted to 2 mg/kg for administration in nude mice according to clinical practice. The CTD-Lip group received an intraperitoneal injection of 0.7 mg/kg of the drug every two days for two weeks, based on in vitro IC_{50} values and preliminary dose-ranging studies in mice. Body mass and tumor volume were also measured in the mean while. Twenty-four hours after the final administration, euthanasia was performed, and tumors as well as main organs (heart, liver, spleen, lungs, and kidneys) were collected. These samples were washed with normal saline, placed on filter paper to remove surface water absorption, and stored at −20 °C or in a solution containing 4% paraformaldehyde for subsequent experiments and analysis.

The tumor mass was measured, and the tumor inhibition rate of the CTD-Lip group and the cisplatin group was calculated using the following formula: tumor inhibition rate = (tumor mass of the control group - tumor mass of the experimental group) / tumor mass of the control group ×100%.

2.7. HE staining and TUNEL analysis of tumor tissues

First, the heart, liver, spleen, lung, kidney, and tumor of nude mice were fixed in 4% paraformaldehyde and stored. For histopathological evaluation, formalin-fixed tissues were processed into 4–5 μm paraffin sections and stained with Mayer's hematoxylin and eosin (H&E) (H3136, Sigma-Aldrich, USA) using standard protocols. Apoptosis was assessed via TUNEL assay (11684795910, Roche, Germany), where deparaffinized sections were treated with Proteinase K (20 μg/mL), followed by enzymatic labeling with TdT and fluorescein-dUTP at 37 ℃ for 60 min. Nuclei were counterstained

with DAPI, and TUNEL-positive cells were quantified using the apoptotic index [20,21].

2.8. Hematological and biochemical examinations of mice

Prior to the dissection of mice, orbital blood samples were obtained. A portion of the whole blood was collected and preserved in an anticoagulant tube for subsequent hematological analysis using an automated blood cell analyzer. Subsequently, another portion of blood was collected for biochemical analysis of liver, kidney, and cardiac function indicators using an automated biochemical analyzer. The biochemical analysis encompassed alanine aminotransferase (ALT), aspartate aminotransferase (AST), urea nitrogen (BUN), creatinine (CREA), creatine kinase (CK), and lactate dehydrogenase (LDH).

2.9. Statistical methods

R statistical software (version 4.4.1) was used for analysis. Data were summarized in the form of mean ± standard deviation values. Student's t-test was used to analyze the differences between the two groups. ANOVA and Tukey's post-hoc test were performed to evaluate the significance among the groups. Differences were considered to be statistically significant when $P < 0.05$.

3. Results

3.1. Successful construction and sustained release characteristics of CTD-Lip

Physicochemical characterization revealed a mean particle size of 120.80 ± 0.529 nm with a polydispersity index (PDI) of 0.26 ± 0.001 and zeta potential of −29.9 ± 1.015 mV (Figure 1a–c). The encapsulation efficiency of CTD-Lips was 96.20% (SD: 1.305%), and drug loading was 14.30% (SD: 0.987%). The cumulative release rate of CTD-Lip at 48 h was approximately 60%, while the cumulative release rate of CTD was nearly 100% within 6 h. These results reflect the sustained release nature of liposomes and demonstrate that lipid-based nanoparticles often exhibit prolonged release beyond 48–72 h as reported by prior literature [22] (Figure 1d).

3.2. Enhanced cellular internalization mediated by Lips

Cellular uptake efficiency was evaluated using coumarin-6-loaded liposomes (C6-Lip) in HepG2 cells. Fluorescence microscopy revealed significantly intensified intracellular fluorescence in the C6-Lip group compared to free C6 (Figure 2). Quantitative analysis demonstrated a time-dependent uptake pattern, with fluorescence intensity increasing from 54.84 (SD = 0.461) at initial timepoints to 86.69 (SD = 1.360) at later stages (Figure 2b). Notably, the uptake rate plateaued between 4 h (mean = 82.27, SD = 0.996) and 6 h (mean = 86.69, SD = 1.360), suggesting saturation kinetics ($P < 0.01$, Figure 2b). Statistical comparisons confirmed significantly higher cellular accumulation of C6-Lip versus free C6 across all timepoints (all $P < 0.001$, Figure 2c).

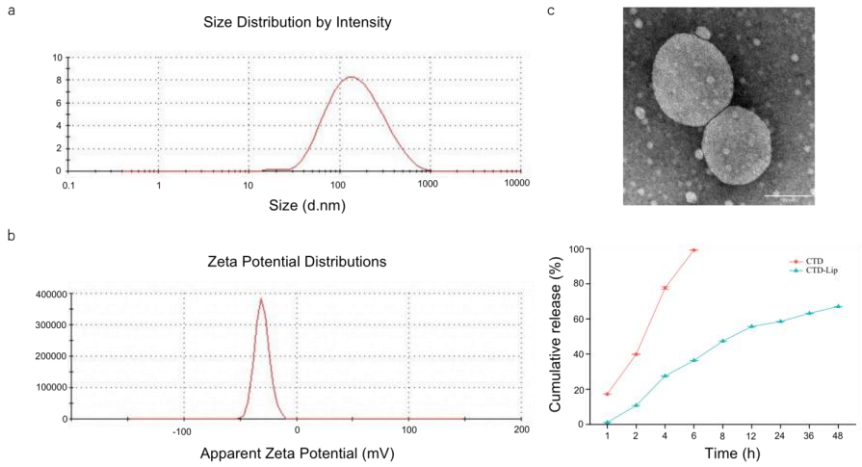

Figure 1. Characterization and in vitro release analysis of CTD-Lip. (a) Determination of particle size distribution. (b) Analysis of zeta potential. (c) Observation of particle morphology of CTD-Lip using transmission electron microscopy (scale bar, 100 nm). (d) Evaluation of in vitro release profiles for both CTD-Lip and free CTD. Data are presented as mean ± standard deviation (SD) (n = 3). CTD: cantharidin, Lip: liposome. For clearer and higher-resolution figures, please refer to the supplementary files.

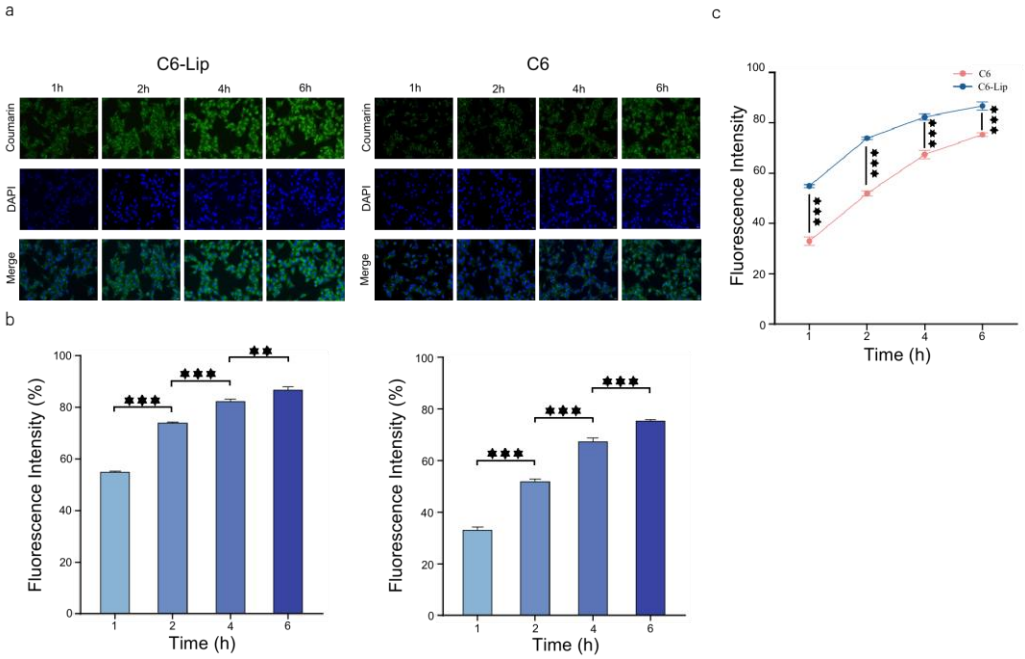

Figure 2. Comparison analysis of cellular uptake of C6-Lip or C6 in HepG2 cells. (a) Comparison of fluorescence intensity of HepG2 cells at different time points upon incubation with C6 Lip (left) and C6 (right) (scale bar: 50 μm). (b) Semi-quantitative analysis results of fluorescence intensity in HepG2 cells incubated with C6-Lip (left) and C6 (right) along with the time flow over time (1–6 h). (c) Statistical analysis of fluorescence intensity difference between C6-Lip and C6. Data are presented as mean ± standard deviation (n = 3). C6: coumarin 6, Lip: liposome. *P < 0.05, **P ≤ 0.01, ***P ≤ 0.001.

3.3. Potentiated anticancer activity of CTD-Lip

Both free CTD and CTD-Lip demonstrated inhibitory effects on HepG2 cell proliferation 24 h post-administration, with a gradual decrease in cell viability observed as the dose increased. The IC_{50} value of CTD-Lip (1.415 μg/mL) was significantly lower than that of CTD (4.971 μg/mL) (Figure 3b). Notably, the blank liposome group exhibited no discernible cytotoxic effects within the designated concentration range, indicating their favorable safety profile (Figure 3a, left). These findings highlight the significant enhancement of cytotoxicity against tumor cells by CTD-Lip (Figure 3a and b).

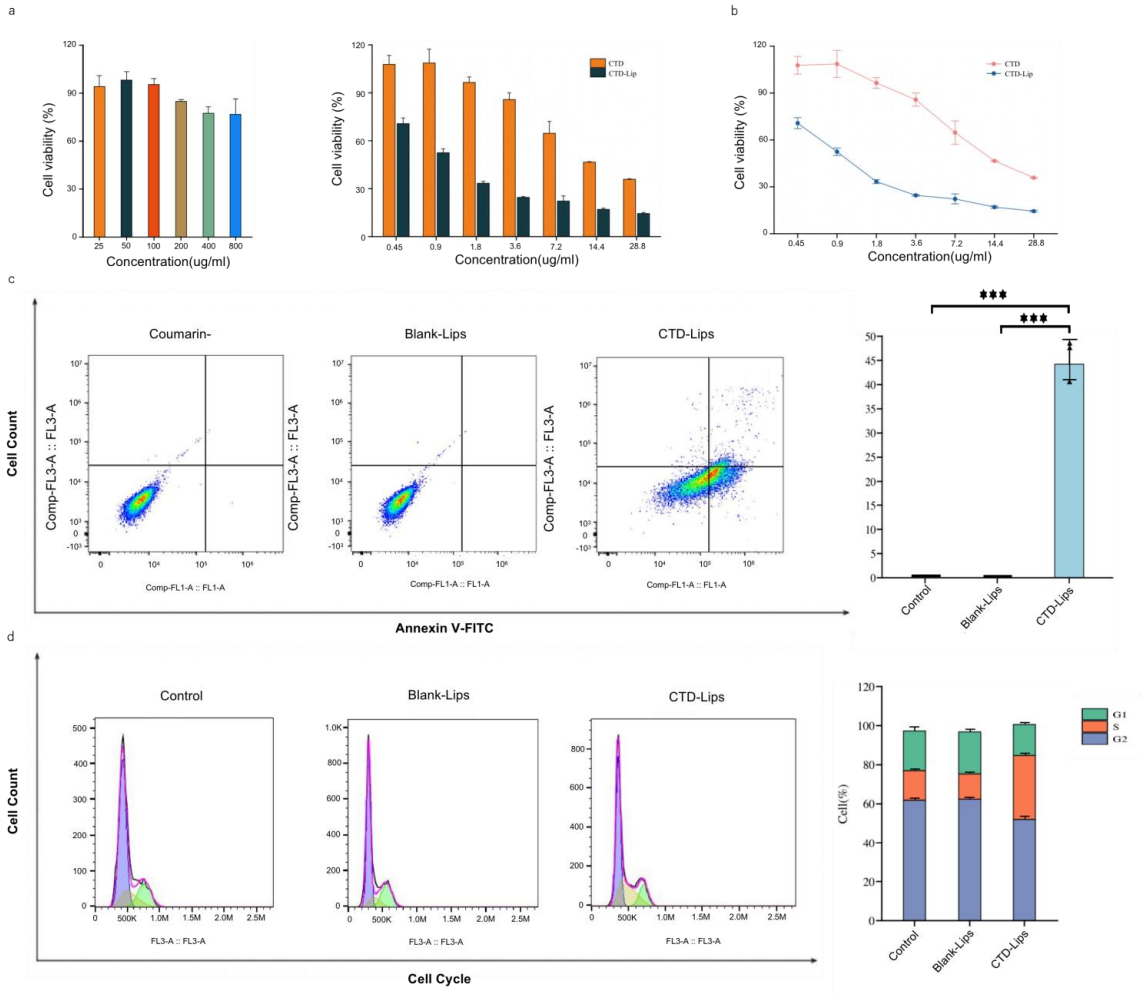

Figure 3. Analysis of toxic effects of CTD, CTD-Lips, and blank Lips on HepG2 cells. (a) Evaluation of HepG2 cell toxicity through cell viability analysis after co-cultivation with different concentrations of liposome (left), CTD-Lip and CTD drugs (right, n = 3, incubation time: 24 h). (b) Assessment of HepG2 cell toxicity following exposure to blank Lips (24 h) with different concentrations. (c) Investigation into the effect of CTD-Lips (1.42 μg/mL) treatment on the cell cycle in HepG2 cells (24 h). (d) Examination of the influence of CTD-Lips (1.42 μg/mL) treatment on apoptosis in HepG2 cells (48 h). Data are presented as mean ± standard deviation (n = 6). CTD: cantharidin, Lip: liposome. *P < 0.05, **P ≤ 0.01, ***P ≤ 0.001.

Figure 3c shows that the apoptosis rate in the CTD-Lips group showed a substantial increase ($P < 0.001$), accompanied by an elevated percentage of cells in S phase ($P < 0.01$). Conversely, there was no notable difference in apoptosis rates between blank-Lips and control groups for HepG2 cells, suggesting minimal impact on apoptosis from blank liposomes. Therefore, it can be speculated that CTD-Lips effectively promote apoptosis and induce cell cycle arrest at S phase while inhibiting cell proliferation (Figure 3c and d).

3.4. Improvement of anti-cancer efficacy and biosafety profile from CTD-Lip in vivo

In xenograft models, CTD-Lip treatment achieved superior tumor growth inhibition (62.4%) compared to cisplatin (DDP) controls (Figure 4a–c). Tumor volume from the control group reached 299.69 mm^3 (SD = 77.20), while that from the CTD-Lip-treated group was 26.37 mm^3 (SD = 4.97), which was even lower than that from the cisplatin (DDP)-treated group (mean = 91.33 mm^3, SD = 24.37) (Figure 4c). Moreover, CTD-Lip treatment did not significantly impact the body weight of nude mice (Figure 4d).

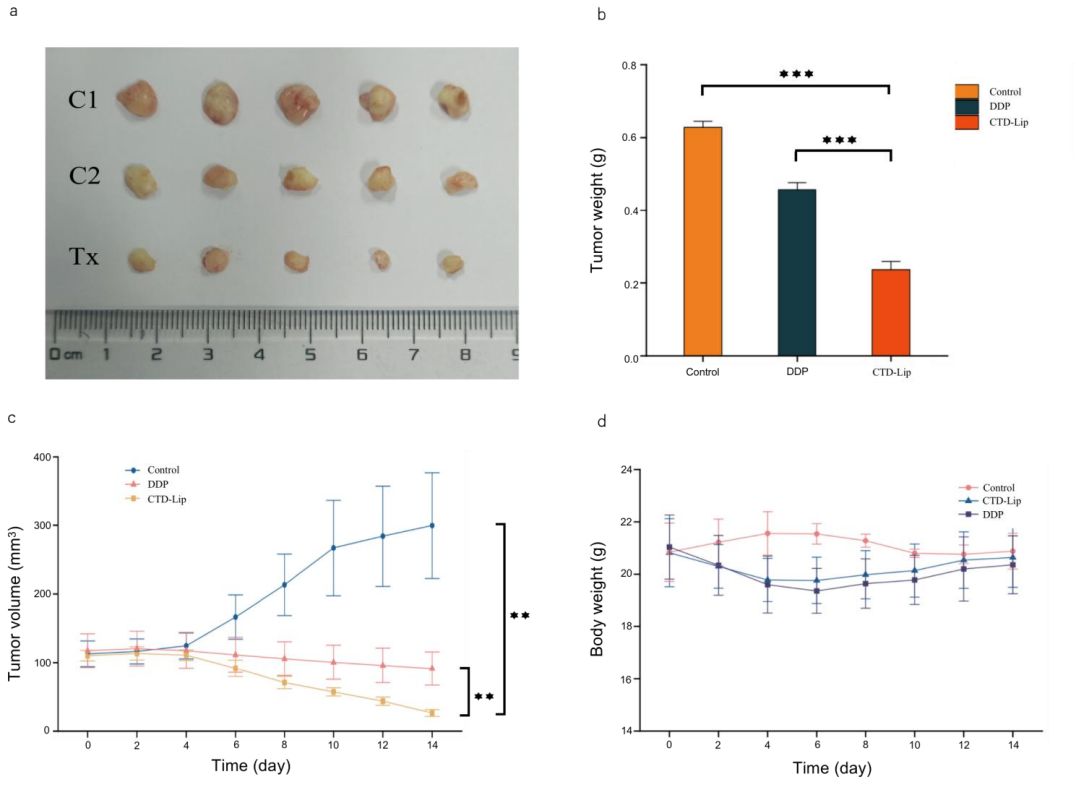

Figure 4. Analysis of the in vivo anticancer efficacy of CTD-Lips. (a) Tumor volume of nude mice, depicting the response across different treatment groups. (b) Comparison of tumor weights observed after therapy among different treatment groups. (c) Tumor growth curves illustrating the progression in nude mice treated with various regimens. (d) Weight change curves showcasing alterations in body weight within different treatment groups (n = 5). C1: control group; C2: DDP-treated group; Tx: CTD-Lip-treated group. Data are presented as mean ± standard deviation (n = 5). CTD: cantharidin, DDP: cisplatin, Lip: liposome. *$P < 0.05$, **$P \leq 0.01$, ***$P \leq 0.001$.

HE staining of organ and tumor tissues was observed to analyze the therapeutic effect in vivo (Figure 5). The revealed cell damage, including reduced cell volume and nuclear rupture, was found in tumor tissues (Figure 6a). Both the positive control group, treated with DDP, and the CTD-Lip group exhibited such cell damage, indicating the anti-tumor effects of CTD-Lip (Figure 6a). However, no noticeable pathological damage was observed in organ tissue (Figure 5). Additionally, Figure 5c displayed strong green fluorescence in both the DDP group and the CTD-Lip group, suggesting a substantial amount of tumor cell apoptosis. Notably, the CTD-Lip group showed even stronger fluorescence intensity, highlighting its ability to effectively promote tumor cell apoptosis (Figure 6b).

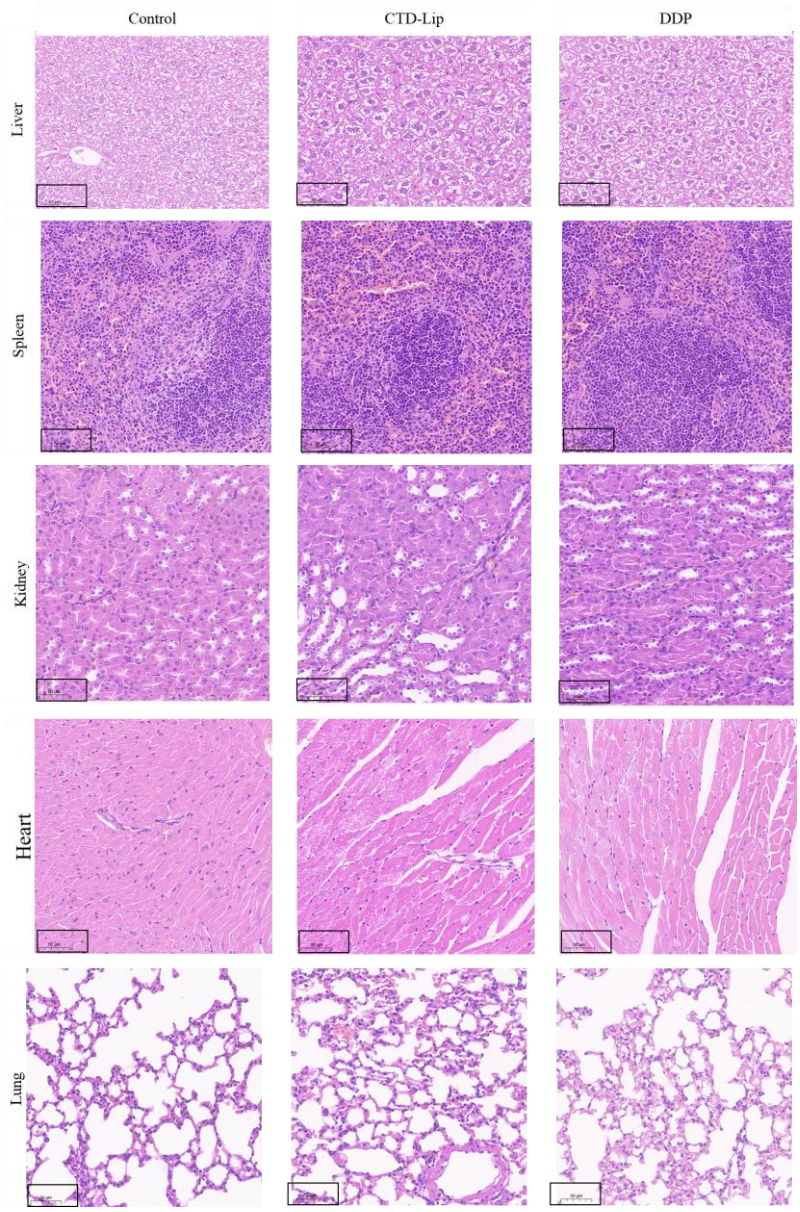

Figure 5. Analysis of tumor and major organ histopathology using HE staining in nude mice. HE staining images for heart, liver, spleen, lung, and kidney (scale bar: 50 μm) depicting major organ histology in nude mice across different treatment groups from control, CTD-Lip (0.7 mg/kg), and DDP (2 mg/kg).

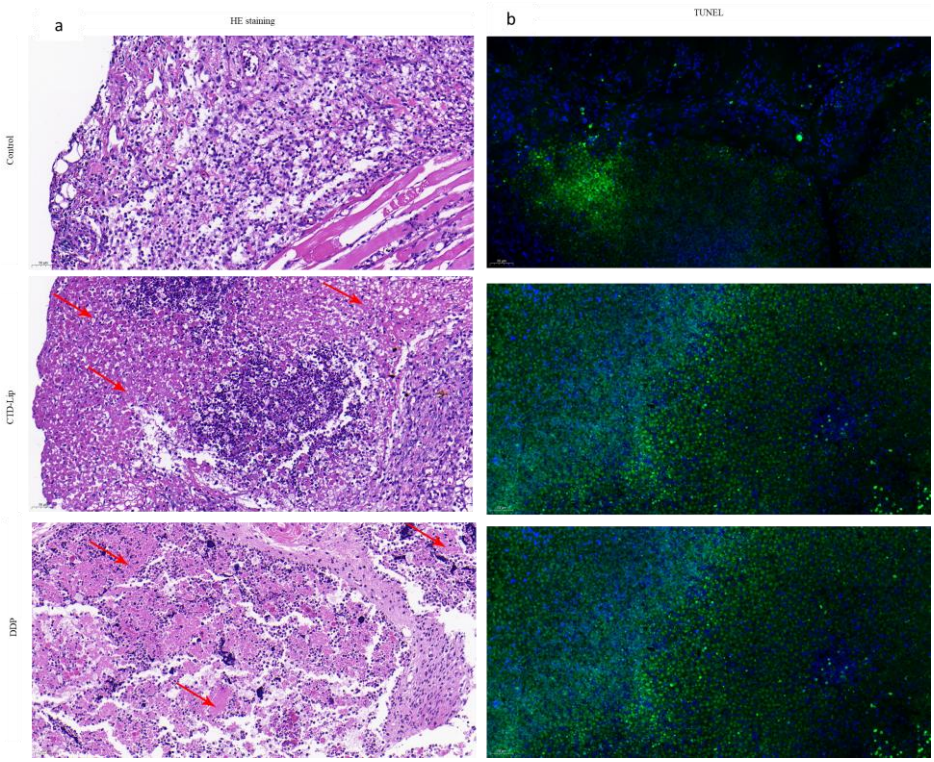

Figure 6. Analysis of tumor and major organ histopathology using HE staining, and detection of apoptotic cells through TUNEL assay in nude mice. (a) HE staining images (scale bar: 50 μm) illustrating tumor histology in nude mice subjected to various treatments: control, CTD-Lip (0.7 mg/kg), and DDP (2 mg/kg). (b) Fluorescent images (scale bar: 50 μm) demonstrating apoptosis of tumor tissue cells detected by TUNEL assay under control, CTD-Lip (0.7 mg/kg), and DDP (2 mg/kg) treatments. CTD: cantharidin; HE: hematoxylin and eosin; Lip: liposome.

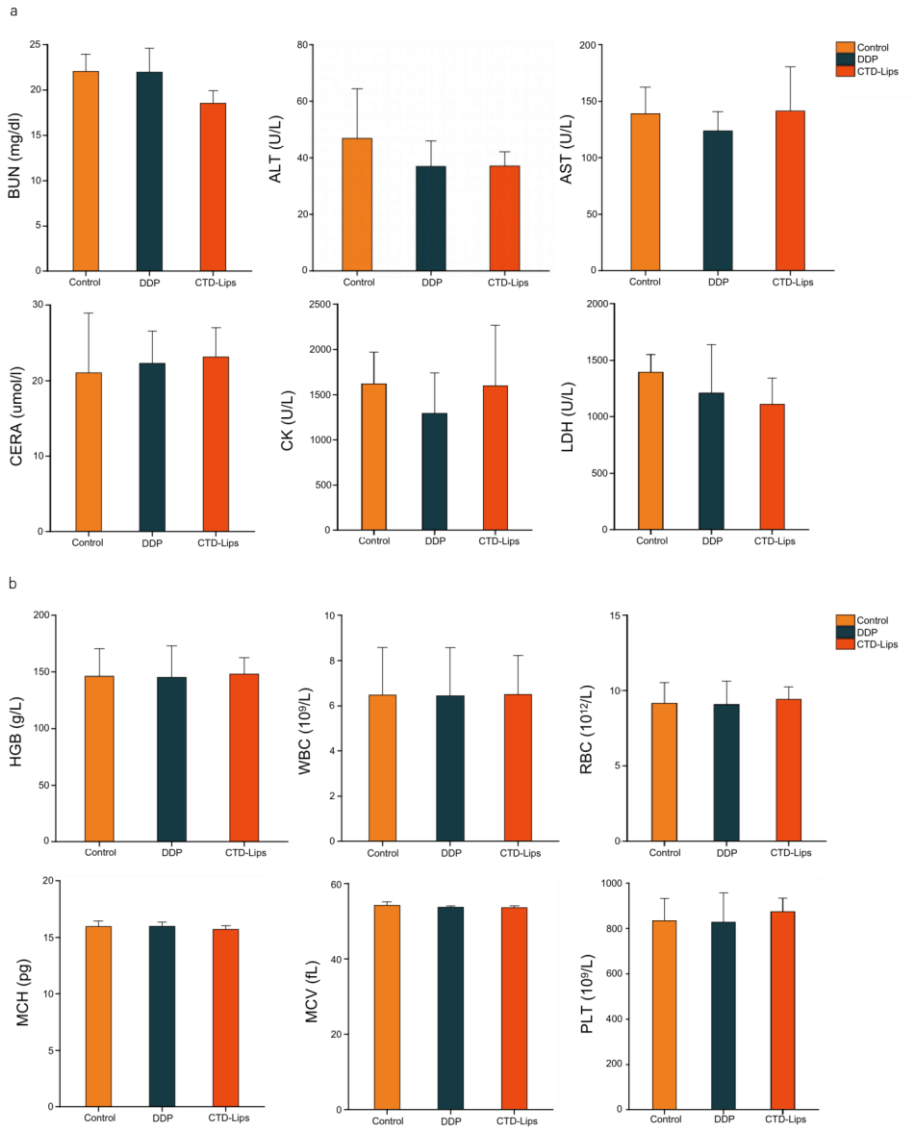

Figure 7. Detection of hematological and blood biochemical indicators in nude mice. (a) Blood biochemical indexes in different groups of nude mice after treatment. (b) Hematological parameters in different groups of nude mice after treatment. Data are presented as mean ± standard deviation (n = 3). ALT: alanine transaminase, AST: aspartate transaminase, BUN: blood urea nitrogen, CERA: continuous erythropoietin receptor activator, CK: creatine kinase, CTD: cantharidin, HGB: hemoglobin, LDH: lactate dehydrogenase, MCH: mean corpuscular hemoglobin, MCV: mean corpuscular volume, PLT: platelet, RBC: red blood cells, Lip: liposome, WBC: white blood cell.

Hematological parameters indicated no significant differences between the control group and either the positive drug or CTD-Lip group, and all index values remained within normal ranges (Figure 7). This finding confirmed that the prepared liposomes had no evident toxic side effects and exhibited good biological safety. Meanwhile, there were intact morphologies and structures observed in visceral tissue sections across all groups without any noticeable pathological damage (Figure 5).

4. Discussion

Cantharidin, extracted from *Cantharis*, serves as the primary component in anti-cancer drugs. It is widely utilized in clinical antitumor therapy [23,24] and exhibits remarkable antitumor activity against various cancers. Particularly, cantharidin demonstrates a positive therapeutic effect on liver cancer [16]. However, its application is hindered by poor water solubility, low bioavailability, and high toxicity. In recent years, numerous derivatives of cantharidin-related drugs have been developed to mitigate their cytotoxicity [25]. To overcome these challenges in the clinical use of cantharidin, this study introduces an innovative dosage form: liposomes containing cantharidin. This formulation addresses issues such as the fat-soluble nature of cantharidin's active ingredient, leading to poor water solubility and rapid elimination after administration. Moreover, it reduces nephrotoxicity while cholesterol and egg yolk lecithin enhance the solubility of fat-soluble active ingredients in the oil phase. These advancements provide a prerequisite and guarantee for developing highly efficient nano-drug delivery systems without potentially toxic nanocarrier materials while ensuring good biocompatibility.

In this study, cantharidin was formulated into liposomes (Lips) with a nanoscale particle size of approximately 120 nm, which is crucial for effective anti-tumor therapy. If the particles are too small, they will be rapidly eliminated by the kidneys; if their size exceeds 300 nm, they are easily captured by the reticuloendothelial system (RES), hindering their ability to reach the target site [26]. Additionally, our study demonstrated that CTD-Lip exhibited superior sustained release performance compared to CTD alone, with a cumulative release rate of 60% over 48 h versus 100% over 6 h. However, an observation on the 100% release time as well as the release kinetic mode should be arranged in a future study. Consequently, upon administration into the body, CTD-Lip is more likely to penetrate cells due to its enhanced permeability and retention effect (EPR), resulting in prolonged drug activity. Moreover, when exerting cytotoxic effects on liver cancer cells at equivalent efficacy levels, lower concentrations of cantharidin liposomes are required with reduced toxicity. This approach enhances efficiency while minimizing harm. Notably, treatment of HepG2 cells with CTD-Lip primarily induced cell cycle arrest in the S phase, suggesting inhibition of DNA synthesis and promotion of apoptosis in hepatocellular carcinoma cells [27].

Numerous studies have proposed mechanisms by which cantharidin exhibits anti-tumor activity, namely by affecting the synthesis of RNA and DNA to induce DNA damage and apoptosis and suppress cell proliferation [13,14]. Namely, CTD functions as a protein phosphatase 2A (PP2A) inhibitor to induce DNA damage [13]. Moreover, CTD has also been observed to enhance chemosensitivity in HCC cells by upregulating the expression of KDM4A, leading to H3K36me3-dependent DNA damage in HCC [14].

Cisplatin, also known as cis-diamminedichloroplatinum (DDP), is widely used for the treatment of various human tumors, including ovarian cancer, breast cancer, and brain cancer [28-31]. Cisplatin treatment can also induce DNA damage, inhibit cell proliferation, and promote cell apoptosis [32]. This treatment modality exhibits a comparable anti-cancer effect to CTD and is commonly employed in the management of HCC via transcatheter arterial chemoembolization (TACE) [33]. Therefore, we conducted a comparative analysis of the therapeutic efficacy between DDP and CTD-Lip, which demonstrated a significant advantage of CTD-Lip in inhibiting tumor growth. Both the measurement of tumor volume and the results obtained from apoptosis staining using TUNEL cells indicated that CTD-Lip exhibited superior effectiveness in inducing apoptosis of tumor cells. Moreover, considering the resistance often observed in HCC patients toward DDP treatment, we believe that combining CTD-Lip with DDP

intervention can effectively enhance the prognosis for these patients. Additionally, it has been reported that interventional therapy involving DDP increases sensitivity to its treatment among HCC patients [33]. However, subsequent investigations are also necessary to incorporate comprehensive pharmacokinetic profiling, which will enable the direct quantification of bioavailability and further validate the current findings.

HE staining performed on animal tissues revealed no significant toxicity associated with CTD-Lip administration compared to both the control group and the DDP-treated group. Furthermore, through small animal weight tracking experiments, we observed a slight increase in body weight among mice treated with CTD-Lip as compared to those treated with DDP (although this difference was not statistically significant). Therefore, our findings suggest that CTD-Lip effectively mitigates the toxicity associated with CTD administration; when combined with DDP interventional therapy, it holds great potential for improving the prognosis of HCC patients.

However, due to the natural origin of cantharidin, its solubility is extremely poor, making it challenging to dissolve in cold water. Even if it exhibits slight solubility in hot water, achieving accurate quantitative dissolution remains difficult. Consequently, the experimental group of nude mice did not incorporate the free cantharidin group. These limitations hinder the direct utilization of cantharidin for anti-cancer treatment. This is also the reason why this study seeks new drug delivery methods and establishes CTD-Lip. Moreover, the in vitro drug release assessment was conducted over 48 h, precluding the determination of the complete release profile. Consequently, the associated kinetic model analysis is based on this initial release phase. Furthermore, detailed solid-state characterizations, such as differential scanning calorimetry, and long-term stability data were not included. These aspects should be addressed in future work to complement the present findings.

5. Conclusions

This study optimized the process to prepare liposomes containing cantharidin. The novel formulation not only enhances drug solubility and cellular uptake but also demonstrates superior antitumor efficacy compared to conventional cisplatin, while markedly reducing systemic toxicity. These findings position CTD-Lips as a promising therapeutic alternative for HCC patients, particularly those developing resistance to current standard treatments.

Author contributions

Conceptualization, YSL; software, RHD, JD and MJC; validation, RHD, JD, MJC, CXH, HL, ZLL and YSL; formal analysis, RHD, JD, MJC, CXH, HL, ZLL and YSL; investigation, RHD, JD, MJC, CXH, SLG, RCL, RHY, HL, ZLL and YSL; resources, ZLL and YSL; data curation, RHD, JD, MJC, CXH, SLG, RCL, RHY, HL, ZLL and YSL; writing—original draft preparation, RHD, JD, MJC, CXH, ZLL and YSL; writing—review and editing, HL, ZLL and YSL; visualization, RHD, JD, MJC, HL, ZLL and YSL; supervision, YSL and ZLL; project administration, YSL; funding acquisition, ZLL and YSL. All authors have read and agreed to the published version of the manuscript.

Use of Generative-AI tools declaration

The authors declare they have not used Artificial Intelligence (AI) tools in the creation of this

article.

Acknowledgments

This research was funded by The Natural Science Foundation of Guangdong Province, China (2019A1515012118, 2023A1515010388, 2025A1515012376) and Scientific research capacity improvement project of key construction disciplines in Guangdong Province, China (2024ZDJS129) and Huizhou Science and Technology Project, China(2022CZ010414).

Conflict of interest

The authors declare no conflicts of interest in this paper.

References

1. Benson AB, D'Angelica MI, Abbott DE, et al. (2021) Hepatobiliary cancers, version 2.2021, NCCN clinical practice guidelines in oncology. *J Natl Compr Canc Netw* 19: 541–565. https://doi.org/10.6004/jnccn.2021.0022
2. Pan MS, Cao J, Fan YZ (2020) Insight into norcantharidin, a small-molecule synthetic compound with potential multi-target anticancer activities. *Chin Med* 15: 55. https://doi.org/10.1186/s13020-020-00338-6
3. Zheng LH, Bao YL, Wu Y, et al. (2008) Cantharidin reverses multidrug resistance of human hepatoma HepG2/ADM cells via down-regulation of P-glycoprotein expression. *Cancer Lett* 272: 102–109. https://doi.org/10.1016/j.canlet.2008.06.029
4. Su CC, Lee KI, Chen MK, et al. (2016) Cantharidin induced oral squamous cell carcinoma cell apoptosis via the JNK-regulated mitochondria and endoplasmic reticulum stress-related signaling pathways. *PloS One* 11: e0168095. https://doi.org/10.1371/journal.pone.0168095
5. Xu MD, Liu L, Wu MY, et al. (2018) The combination of cantharidin and antiangiogenic therapeutics presents additive antitumor effects against pancreatic cancer. *Oncogenesis* 7: 94. https://doi.org/10.1038/s41389-018-0102-2
6. McCluskey A, Bowyer MC, Collins E, et al. (2000) Anhydride modified cantharidin analogues: Synthesis, inhibition of protein phosphatases 1 and 2A and anticancer activity. *Bioorg Med Chem Lett* 10: 1687–1690, https://doi.org/10.1016/s0960-894x(00)00323-1
7. Li HC, Xia ZH, Chen YF, et al. (2017) Cantharidin inhibits the growth of triple-negative breast cancer cells by suppressing autophagy and inducing apoptosis in vitro and in vivo. *Cell Physiol Biochem* 43: 1829–1840. https://doi.org/10.1159/000484069
8. Pan Y, Zheng Q, Ni W, et al. (2019) Breaking glucose transporter 1/pyruvate kinase M2 glycolytic loop is required for cantharidin inhibition of metastasis in highly metastatic breast cancer. Front Pharmacol 10: 590. https://doi.org/10.3389/fphar.2019.00590
9. Chen CC, Chueh FS, Peng SF, et al. (2019) Cantharidin decreased viable cell number in human osteosarcoma U-2 OS cells through G_2/M phase arrest and induction of cell apoptosis. Biosci Biotechnol Biochem 83: 1912–1923. https://doi.org/10.1080/09168451.2019.1627182

10. Zhu M, Shi X, Gong Z, et al. (2020) Cantharidin treatment inhibits hepatocellular carcinoma development by regulating the JAK2/STAT3 and PI3K/Akt pathways in an EphB4-dependent manner. *Pharma Res* 158: 104868. https://doi.org/10.1016/j.phrs.2020.104868
11. Song M, Wang X, Luo Y, et al. (2020) Cantharidin suppresses gastric cancer cell migration/invasion by inhibiting the PI3K/Akt signaling pathway via CCAT1. *Chem-Biol Interact* 317: 108939. https://doi.org/10.1016/j.cbi.2020.108939
12. Feng IC, Hsieh MJ, Chen PN, et al. (2018) Cantharidic acid induces apoptosis through the p38 MAPK signaling pathway in human hepatocellular carcinoma. *Environ Toxicol* 33: 261–268. https://doi.org/10.1002/tox.22513
13. Zhou H, Xu J, Wang S, et al. (2018) Role of cantharidin in the activation of IKKα/IκBα/NF-κB pathway by inhibiting PP2A activity in cholangiocarcinoma cell lines. *Mol Med Rep* 17: 7672–7682. https://doi.org/10.3892/mmr.2018.8860
14. Wei C, Deng X, Gao S, et al. (2022) Cantharidin inhibits proliferation of liver cancer by inducing DNA damage via KDM4A-dependent histone H3K36 demethylation. *Evid Based Complement Alternat Med* 2022: 2197071. https://doi.org/10.1155/2022/2197071
15. Zou JJ, Zhang SQ, Feng RX (2002) The toxicity and pharmacokinetics of cantharidin. *J China Pharm Univ* 33: 393–396.
16. Zhong M, Xiao N, Li C, et al. (2025) Nanomedicine in cancer diagnosis and therapeutics. *AIMS Mol Sci* 12: 411–437. https://doi.org/10.3934/molsci.2025023
17. Zhang J, Peng Y, Hu S, et al. (2025) Therapeutic application of curcumin and its nanoformulation in dentistry: Opportunities and challenges. *AIMS Mol Sci* 12: 148–172. https://doi.org/10.3934/molsci.2025010
18. Soni PK, Saini TR (2021) Formulation design and optimization of cationic-charged liposomes of brimonidine tartrate for effective ocular drug delivery by design of experiment (DoE) approach. *Drug Dev Ind Pharm* 47: 1847–1866. https://doi.org/10.1080/03639045.2022.2070198
19. Qualls ML, Hagewood H, Lou J, et al. (2022) Bis-boronic acid liposomes for carbohydrate recognition and cellular delivery. *Chembiochem* 23: e202200402. https://doi.org/10.1002/cbic.202200402
20. Onica EC, Dumitru CS, Zara F, et al. (2025) Pentachroma O-H: A five-color histological staining method for enhanced intestinal tissue analysis. *Int J Mol Sci* 26: 10811. https://doi.org/10.3390/ijms262210811
21. Mantle P, Upadhyay R, Herman D, et al. (2025) Renal apoptosis in male rats induced by extensive dietary exposure to ochratoxins. *Int J Mol Sci* 26: 4553. https://doi.org/10.3390/ijms26104553
22. Patil K, Gujarathi N, Sharma C, et al. (2024) Quality-by-design-driven nanostructured lipid scaffold of apixaban: Optimization, characterization, and pharmacokinetic evaluation. *Pharmaceutics* 16: 910. https://doi.org/10.3390/pharmaceutics16070910
23. Zhang D, Xu X, Wei Y, et al. (2022) Prognostic role of DNA damage response genes mutations and their association with the sensitivity of olaparib in prostate cancer patients. *Cancer control* 29: 1–16. https://doi.org/10.1177/10732748221129451
24. Zhou J, Ren Y, Tan L, et al. (2020) Norcantharidin: Research advances in pharmaceutical activities and derivatives in recent years. *Biomed Pharmacother* 131: 110755, https://doi.org/10.1016/j.biopha.2020.110755

25. Yan J, Deng XL, Ma SQ, et al. (2023) Cantharidin suppresses hepatocellular carcinoma development by regulating EZH2/H3K27me3-dependent cell cycle progression and antitumour immune response. *BMC Complement Med Ther* 23: 160. https://doi.org/10.1186/s12906-023-03975-0
26. Xu Y, Wang M, Ning S, et al. (2022) Development of glycyrrhetinic acid and folate modified cantharidin loaded solid lipid nanoparticles for targeting hepatocellular carcinoma. *Molecules* 27: 6786. https://doi.org/10.3390/molecules27206786
27. Naz F, Wu Y, Zhang N, et al. (2020) Anticancer attributes of cantharidin: Involved molecular mechanisms and pathways. *Molecules* 25: 3279. https://doi.org/10.3390/molecules25143279
28. Dasari S, Tchounwou PB (2014) Cisplatin in cancer therapy: molecular mechanisms of action. *Eur J Pharm* 740: 364–378. https://doi.org/10.1016/j.ejphar.2014.07.025
29. Koch M, Krieger ML, Stölting D, et al. (2013) Overcoming chemotherapy resistance of ovarian cancer cells by liposomal cisplatin: molecular mechanisms unveiled by gene expression profiling. *Biochem Pharm* 85: 1077–1090. https://doi.org/10.1016/j.bcp.2013.01.028
30. Silver DP, Richardson AL, Eklund AC, et al. (2010) Efficacy of neoadjuvant Cisplatin in triple-negative breast cancer. *J Clin Oncol* 28: 1145–1153. https://doi.org/10.1200/jco.2009.22.4725
31. Zhang C, Nance EA, Mastorakos P, et al. (2017) Convection enhanced delivery of cisplatin-loaded brain penetrating nanoparticles cures malignant glioma in rats. *J Control Release* 263: 112–119. https://doi.org/10.1016/j.jconrel.2017.03.007
32. Basu A, Krishnamurthy S (2010) Cellular responses to cisplatin-induced DNA damage. *J Nucleic Acids*. https://doi.org/10.4061/2010/201367
33. Sato R, Moriguchi M, Saiga A, et al. (2024) No lipiodol, no beads-another transcatheter arterial chemoembolization (TACE) with fine cisplatin powder and porous gelatin particles for TACE-naïve, multifocal, up-to-seven out hepatocellular carcinoma. *Cancer Med* 13: e7446. https://doi.org/10.1002/cam4.7446

AIMS Press